

# BUBBLE DYNAMICS, TWO-PHASE FLOW, AND BOILING HEAT TRANSFER IN MICROGRAVITY

Jacob N. Chung  
School of Mechanical and Materials Engineering  
Washington State University  
Pullman, WA 99164-2920

519.09  
202.18.44

## ABSTRACT

608

The objective of the research is to study the feasibility of employing an external force to replace the buoyancy force in order to maintain nucleate boiling in microgravity. We have found that a bulk velocity field, an electric field and an acoustic field could each play the role of the gravity field in microgravity. Nucleate boiling could be maintained by anyone of the three external force fields in space.

## INTRODUCTION

The thermo-fluid dynamics of a two-phase system in microgravity encompasses a wide range of complex phenomena that are not well understood for engineering design to proceed. Therefore, there is an urgent need to explore these phenomena for future spacecraft design and space mission. Predicting the two-phase flow and boiling heat transfer phenomena under microgravity environment requires a thorough understanding of a multitude of fundamental physical processes including bubble dynamics, fluid dynamics, heat transfer, and interfacial transport. Significant gains in microgravity boiling science may result from investigating both the complexities of these phenomena in isolation and when acting in concert. The current research concentrates on the bubble nucleation, bubble dynamics and heat transfer mechanism under microgravity. Specifically, we intend to study the transport mechanisms when the dominance of gravity field is replaced by a bulk velocity field, an electric field or an acoustical field under the microgravity condition.

### I. Bulk Velocity Field

In highly subcooled and high-velocity forced-convection nucleate boiling, bubbles grow, slide, and collapse on the heater surface; therefore, buoyancy is of minimum reliance. In order to obviate the masking effect of buoyancy, our experiment was performed under low-velocity and microgravity conditions such that the physical phenomenon was more clearly recorded by our experimental system.

#### I.1 Experiment

The flow boiling apparatus consists of a pump, preheater, boiling test section, condenser, lighting, and video and data acquisition system. The maximum pump capacity maintained a single-phase mean velocity of  $7.7 \pm 0.1$  cm/s over the heater surface. Due to the physical limitations, the experimental system was open to the atmosphere. The bulk fluid temperature in the experiment was conveniently set to approximately the room temperature. This resulted in a relatively constant subcooling of  $17 \pm 2^\circ\text{C}$  for our experiment. Spectrophotometric grade Freon-113 (1,1,2 trichlorotrifluoroethane 99+ percent) was chosen as the test fluid. Because of the high solubility of dissolved gases in Freon-113 a typical degassing procedure was followed. Data acquisition was performed at 100 Hz for 500 scans: Three seconds of data were recorded before the release to obtain the 1g data, and two seconds of data recorded after the release, which captured the microgravity portion and the deceleration. A semitransparent, 400-Å-thick gold-film heater ( $2.54\text{cm} \times 2.54\text{cm}$ ) was built and used in the experiment. This heater design allowed us to maintain a relatively constant heat flux during the experiment and also provided the average surface temperature. The uncertainty in the heater resistance, surface temperature, and heat flux are  $\pm 0.00148$  ohms,  $\pm 1.16^\circ\text{C}$ , and  $\pm 380$  W/m<sup>2</sup>, respectively. This resulted in an uncertainty in heat transfer coefficient of  $\pm 96$  W/m<sup>2</sup> K.

## I.2 Results and Discussion

**A. The heat transfer coefficient** - The heat transfer coefficients are invariably higher during microgravity for both pool and flow boiling except at the highest heat flux. The present findings for the case of pool boiling are in good agreement (both quantitative and qualitative) with some previously published results (Ref. 1), which showed that nucleate pool boiling heat transfer is enhanced as the buoyancy normal to the heater surface is reduced (including microgravity) and that it is degraded as the buoyancy normal to the heater surface is increased. The next result is the sharp decline in the heat transfer coefficient during microgravity for the highest heat flux case ( $7.58 \times 10^4 \text{ W/m}^2$ ). The forced flow only delayed the drop in heat transfer coefficient. The drop in the heat transfer coefficient is thought to have been caused by the drying-up of some portion of the heater surface due to the formation of vapor slugs, which stuck to the surface. The forced flow lost its effectiveness when the vapor agglomerates grew to a certain size and this will be further verified later in the flow visualization study.

Owing to the fact that the forced velocity is constant in all the cases, it is apparent that the forced convection is only effective for the lowest heat flux case ( $2.88 \times 10^4 \text{ W/m}^2$ ), whereas for the other cases the differences in heat transfer coefficient are negligible between pool and forced convection boiling. For the lowest heat flux, the differences in heat transfer coefficient grew even larger during microgravity, which is believed to be due to the ability of the flow to prevent the formation of vapor agglomerates and to maintain single and sliding bubbles. For the other cases, the heating is so high that the bubbles merge into vapor slugs before the flow can move them. The flow visualization, presented later, will also confirm the above-suggested mechanism for the forced-convection boiling.

**B. Visualization study** - Based on a side-by-side comparison between pool and forced-convection boiling flow patterns in the vicinity of the heater surface for heat fluxes ranging from  $2.88 \times 10^4$  to  $7.5 \times 10^4 \text{ W/m}^2$ , we found the following general trends after examining the visualization figures. During microgravity pool boiling, the bubbles did not rise off the heater surface, and as a result, they coalesced to form what might be called "vapor agglomerates." These large bubbles of various shapes have very rough surfaces and tend to cover up the heater surface, which appeared to cause some portions of the surface to become unwetted during the trailing portion of microgravity. The drying-up of the surface due to vapor agglomerates contributed to the drop in heat transfer coefficient for the heat flux of  $7.58 \times 10^4 \text{ W/cm}^2$ , as discussed above. Therefore, under microgravity the bubble swarm of terrestrial boiling was, in general, replaced by bubble slugs and chunk. The average size of the bubbles was seen to increase with the heat fluxes.

The second finding is concerned with the differences between pool and forced convection boiling under microgravity. With forced flows, the bubbles experienced a shear force along the flow direction. In the absence of gravity, the bubble dynamics depends on the balance between the drag due to the forced flow and the surface tension. The surface tension force would prevail if the contact area between the bubble and the heater surface is larger than the bubble frontal surface area experiencing the forced flow, otherwise the drag force would dominate. For the former, a hemispherical bubble would tend to stick to the surface while a spherical bubble, which belongs to the latter case, would most likely slide on the heater surface. Based on the visualization photographs, we found that for medium to high heat fluxes, the coalesced vapor agglomerates tend to form hemispherical or dome shapes with large base areas as a result of rapid vapor generation. Therefore at medium and high heat fluxes ( $4\text{-}7 \times 10^4 \text{ W/m}^2$ ) in the vicinity of the heater surface, the surface tension dominated, which left the forced flow with negligible effects on the bubble dynamics and heat transfer. The heat transfer coefficients discussed previously also support this conclusion.

For the lowest heat flux case under microgravity, the two-phase pattern of the forced-convection boiling was fundamentally different from that of the pool boiling. Owing to the low heating rate, the bubbles did not have any opportunity to coalesce and form vapor agglomerates, which resulted in the dominance of the flow drag over the surface tension. Basically, it was found that the bubbles are spherical and most of them are isolated from another. Based on our image analysis, the average individual bubble size was calculated at 1 to 2 mm while those of the vapor chunks were on the order of 1 cm and up. Strong evidence was found that the isolated spherical bubbles were "sliding" on the heater surface. It is our conclusion that the significantly higher heat transfer coefficient for forced-convection boiling than that for pool boiling in microgravity for the lowest heat flux is apparently due to the combination of the prevention of vapor agglomerate formation by the flow and the sliding of individual spherical bubbles on the heater surface.

**C. Implications to space application** - Based on the measured heat transfer coefficient data and the flow visualization, it is reasonable to suggest that for a given heat flux, if the forced-flow field is strong enough to prevent bubble agglomeration and to maintain single and sliding bubbles, subcooled forced-convection nucleate boiling would be a feasible and efficient heat transfer mechanism in microgravity.

## II. ELECTRIC FIELD

The purpose of study in this section is to understand the effects of a dielectrophoretic (DEP) force that is produced by an electric field on the boiling heat transfer in microgravity. The DEP force on a spherical bubble in an electric field is given as

$$\mathbf{F}_{DEP} = 2\pi R^3 \epsilon_l \left( \frac{\epsilon_v - \epsilon_l}{\epsilon_v - 2\epsilon_l} \right) \nabla |\mathbf{E}|^2 \quad (1)$$

where  $R$  is the radius of the bubble,  $\mathbf{E}$  is the strength of the electric field,  $\epsilon_l$  and  $\epsilon_v$  are the dielectric permittivity for the liquid and vapor phase, respectively. The buoyancy force on a bubble is

$$\mathbf{F}_b = \frac{4}{3}\pi R^3 (\rho_l - \rho_v) g \quad (2)$$

where  $\rho_l$  and  $\rho_v$  are densities of the liquid and vapor phase, respectively. The gravitational acceleration is represented by  $g$ . In our design, the DEP force is either pointing in the direction of gravity or against gravity. For the bubbles in the system, a parameter,  $g'_{(b,e)}$ , is defined to delineate the net external force effects.

$$g'_{(b,e)} = b + e, b = \frac{|\mathbf{F}_b|}{|\mathbf{F}_b^*|} \text{ and } e = \pm \frac{|\mathbf{F}_{DEP}|}{|\mathbf{F}_b^*|} \quad (3)$$

In the above  $F_b^*$  is the buoyancy force under terrestrial gravity level. For our experiment  $b$  is either unity or nearly zero representing terrestrial and microgravity conditions, respectively. The plus sign in the definition of  $e$  represents that the electric force is in the direction of earth gravity and the minus sign indicates that the electric force is in the opposite direction of earth gravity. The selected values for  $e$  in our experiment are 0, -1, -0.5 and -0.1.

### II.1 Experiment

A 1.91 cm platinum wire, 0.025 cm in diameter with a resistance between approximately 0.045 $\Omega$  to 0.05 $\Omega$  (depending on the wire temperature) was used as the heater. The heat flux was calculated from the power given to the heater and the heater surface area. The temperature in the heater was measured using the standard resistometry technique.

Two finite-sized, square plates (2.54cm  $\times$  2.54cm) separated by an angle of 13 degrees were used as the electrodes. A 600  $\text{\AA}$  gold film was sputtered on the surface of the plates and was utilized as the electrically conducting surface. Also, two electrode dimensions were used so that a 23kV potential could correspond to both a 1g and a 2g DEP force, thus eliminating the voltage as a variable. The distance from the imaginary intersection for electrode geometry #1 and #2 were 2.0cm and 1.25cm respectively. In order to control whether the DEP force aided or opposed buoyancy, the direction of the buoyancy force was changed relative to the electrodes. This was done because it was much simpler to invert the experiment than to move the electrodes.

The platinum heater wire was placed at the lower edge of the diverging plates. The platinum heater wire was positioned along the equipotential line at zero potential located at the midplane of the two electrodes. This eliminated nearly all of the coupling effects between the wire and the electric field.

A pool boiling test channel constructed of thick aluminum was used with bulk temperature control obtained from surface mounted KAPTON heaters. A temperature controller and a number of series-T thermocouples were used at various locations to control and monitor the fluid temperature. A diaphragm metal bellows was used in conjunction with a thin-film pressure transducer to monitor and control the system pressure. Composite video (30Hz) was used for visualization and the electric potential was generated with a Hipotronics high-voltage DC power pack. FC-72 was used as the working fluid for

this study because it is an insulating dielectric. A degassing procedure was followed according to the 3M Product manual recommendations.

## II.2 Results and discussion

**A. Visualization study** - Video pictures are given in Figure 1 for two-phase bubbly flows around the heater wire under microgravity condition. Therefore the parameter  $b$  was zero and three electric field strengths were investigated which correspond to  $e$  of -0.1, -0.5 and -1. The parameter  $e$  is zero without any electric field. The applied heat flux is  $12.1 \times 10^4$  W/m<sup>2</sup>. A general trend is that the average sizes of the bubbles are decreased as the voltage is increased. Film boiling is actually taking place on the wire in the absence of an electric field under microgravity ( $b=0, e=0$ ). It is apparent from these images that the DEP force did provide a sufficient external force to remove the vapor bubbles from the heater surface. The application of a relatively small DEP force ( $e=-0.1$ ) resulted in a relatively strong enough force to revert the film boiling back to the nucleate boiling.

**B. Critical heat flux** - Many correlations have indicated that the critical heat flux (CHF) depends on  $g^{1/4}$  (Ref. 2). This can be normalized with terrestrial-gravity conditions and written as

$$\frac{Q_c''(g)}{Q_c''(g^*)} = \left( \frac{g}{g^*} \right)^{1/4} \quad (4)$$

Where  $Q_c''$  is the critical heat flux at terrestrial gravity ( $g^*$ ) and variable gravity conditions ( $g$ ) respectively. This assumes that the fluid properties are not significantly influenced by gravity reductions. An analogy can be formed by simply replacing the gravity field ratio ( $g/g^*$ ) in Equation (4) with the  $g'_{(b,e)}$ , the DEP and buoyancy effective gravity, which yields

$$\frac{Q_c''(g_{eq})}{Q_c''(g^*)} = \left( |g'_{(b,e)}| \right)^{1/4} \quad (5)$$

where  $g_{eq}$  is the equivalent acceleration due to all external forces. The need for an absolute value sign in Equation (5) will be explained next.

Experimental CHF data is given in Figure 2 along with the curve based on Equation (5). First, we note that the data point for the microgravity conditions without any electric field ( $g'(b=0,e=0)=0$ ) is closely matched by the point representing a conditions where the terrestrial buoyancy is completely counter balanced by the DEP force ( $g'(b=1,e=-1)=0$ ). Second, the cases of  $g'(b=1,e=-2)=-1$  and  $g'(b=1,e=0)=1$  give similar CHF values. It means that for the wire, a net force downward or upward relative to the wire would not make any difference for the CHF, which explains the absolute value sign in Equation (5). In general, the concept of an effective gravity which represents the net force of all external forces is verified for the case where gravity and DEP force coexist for the boiling system.

## III. ACOUSTIC FIELD

Pool boiling heat transfer experiments from a platinum wire heater in FC-72 liquid were conducted under terrestrial and microgravity conditions, both with and without the presence of a high intensity acoustic standing wave within the fluid.

### III.1. Experiment

The acoustic-driven boiling system consists of an acoustic resonator, a fluid chamber, and a platinum wire heater. A DC power supply, a personal computer with an A/D card, a frequency generator, and an acoustic amplifier are connected to the boiling system. Lighting and video system is also an integral part of the system. The natural frequency of the acoustic resonator and the fluid chamber must be carefully matched. The fluid level in the chamber was adjusted for the highest acoustic pressure amplitude, and the cleanest sinusoidal pressure distribution in the vertical direction. The pressure was measured with a hydrophone. Both the hydrophone and the resonator were carefully calibrated.

The average heater surface temperature was determined from the measurement of the electrical resistance of the wire. The heat flux was estimated by the power dissipated by the heater wire. The temperature stratification of the fluid was eliminated by the mixing due to acoustic streaming and the bulk temperature was measured by a copper-constantine thermocouple. The microgravity environment was obtained in our 0.6-second and 2.1-second drop towers. All experiments were conducted under atmospheric pressure which corresponded to a saturation temperature of 54.5°C for FC-72. The resonator driving frequency was always set at 10.18 kHz. The acoustic pressure amplitude is 2.6 atm. gauge.

### III.2. Results and Discussion

The effects of acoustics on the heat transfer coefficient (HTC) and vapor bubble movement in pool boiling depend on many factors. The properties of the experiment that can be controlled were the heat flux, acoustic pressure amplitude, heater position within the sound field, and the gravity level.

A. Terrestrial Gravity - The placement of the heater within the sound field was shown to be critical. The heater was placed at several positions within the sound field. Specially attention was given to the following heater positions within the sound field: pressure node, pressure antinode, and halfway between the pressure node and antinode where the acoustic force is the highest. The HTC increased when the heater was positioned anywhere within the sound field. However, the HTC had the highest increase when the heater was placed at the acoustic pressure antinode. The minimum increase in the HTC occurred when the heater was at the acoustic pressure node.

Acoustics had the largest effect on the HTC at the inception of boiling and close to burnout. The temperature of the heater surface dropped by approximately 10 degrees Celsius at the inception of boiling. At larger heat fluxes (46.4 W/cm<sup>2</sup>) the surface temperature dropped over 200°C. The most significant finding is that the incipience superheat excursion is eliminated with the acoustic field on. The effects of acoustics on the HTC diminished in the regime of vapor slugs and columns.

B. Microgravity - As shown in Figure 3, the heat transfer is more efficient in the presence of a sound field. Without an acoustic field, the degree of superheat was increased during microgravity. The heater surface temperature remained unaffected, when the system went from terrestrial gravity to microgravity under an acoustic field. Without a sound wave, the vapor bubbles tend to stay on the heater surface during microgravity, which increases the heater surface temperature. The acoustic field helps remove the bubbles during microgravity, which seems to maintain the heater surface temperature at a relatively constant value.

The effect of acoustics on vapor bubbles in pool boiling was investigated by video visualization. When the heater is placed at the acoustic pressure antinode the vapor bubbles were driven toward the pressure node. Only a few bubbles were seen along the heater surface. When the heater was located at the acoustic pressure node the bubbles were levitated around the heater. The vapor bubbles varied in size and they were not equally spaced along the heater. It is reasonable to conclude that it is feasible to maintain nucleate boiling in microgravity by placing the heater wire at the acoustic pressure antinode.

### ACKNOWLEDGMENT

The work was supported by NASA Grant No. NAG3-1387. The author is grateful for the assistance and support of Dr. Fran hiaramionte at the NASA Lewis Research Center. The 3M Company donated the FC72 for our research.

### REFERENCES

1. Merte, H., Jr., Lee, H.S. and Ervin, J.S., Transient Nucleate Pool Boiling in Microgravity - Some Initial Results, Int. Symp. Microgravity Science and Applications, Paper J-5, 1993.
2. Zuber, N., On the Stability of Boiling Heat Transfer, J. Heat Transfer, Vol. 80, 1958, pp. 711-718.

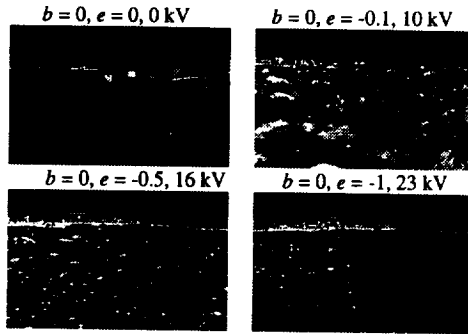


Figure 1 - Microgravity boiling ( $b=0$ ) with various DEP forces ( $e=-1, -0.5, -0.1, 0$ ), Heat Flux =  $12.1 \times 10^4 \text{ W/m}^2$

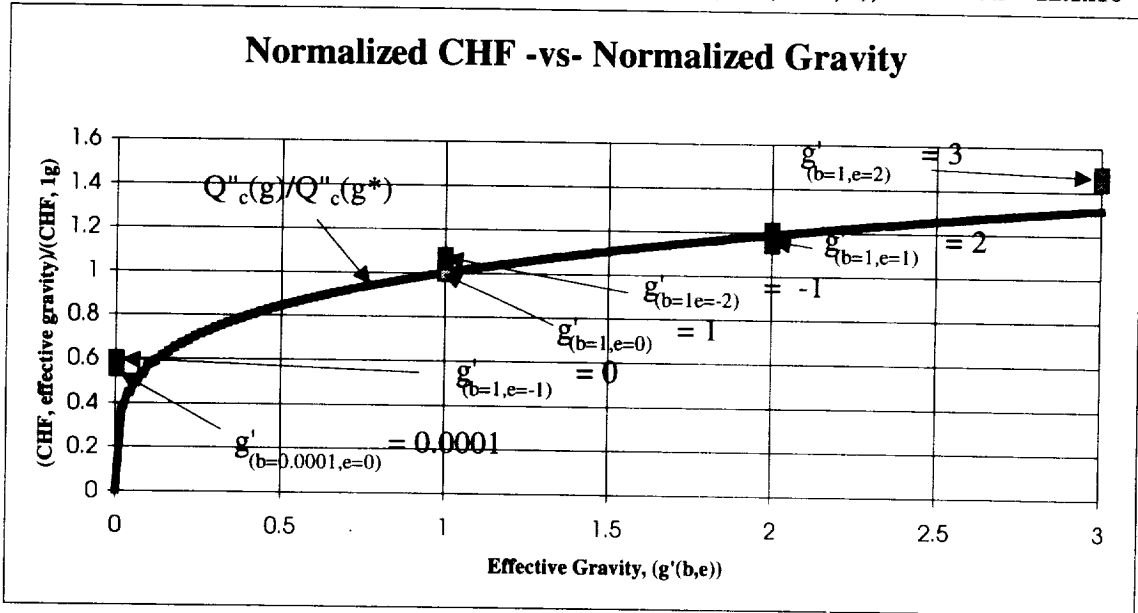


Figure 2 - Normalized CHF -vs- Effective Gravity

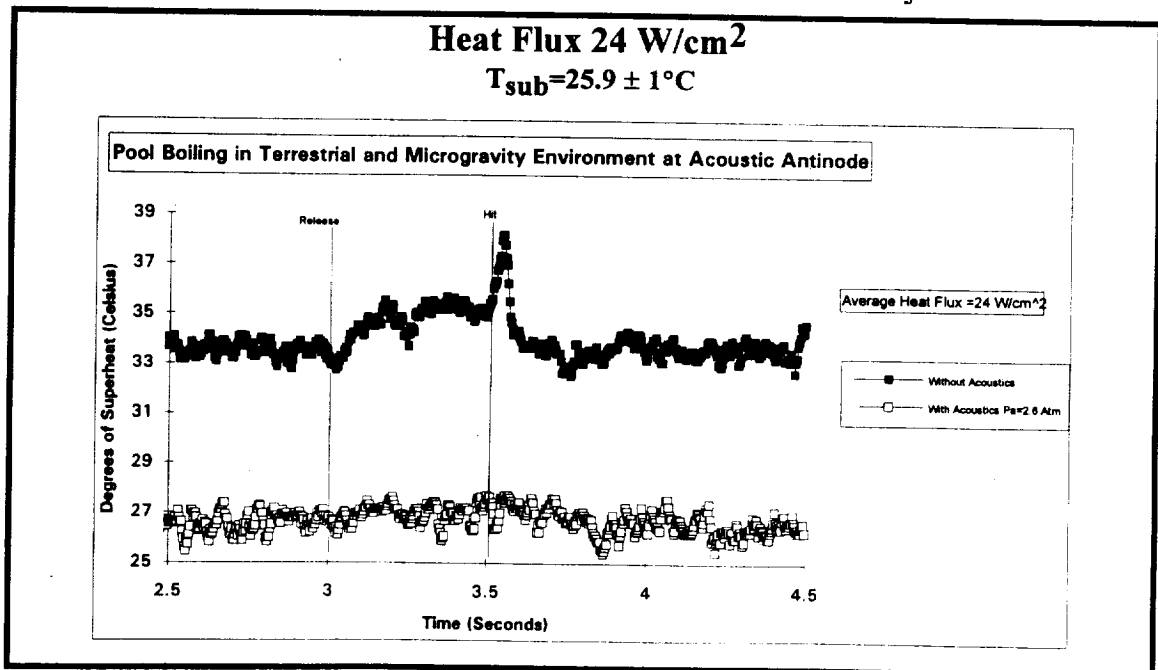


Figure 3